Prognosis prediction in head and neck cancer

Conor Whitley

The University of Liverpool, Department of Physics

Abstract

1 Introduction

Oral squamous cell carcinoma (OSCC) is the sixth most common form of cancer worldwide with a recent increase in incidence reported [1]. The majority of head and neck cancers are squamous cell carcinomas that originate in the upper aerodigestive epithelium and are typically associated with exposure to carcinogens present in tobacco and alcohol [2]. The regions in which head and neck tumours typically develop are anatomically complex and play a vital physiological role in the patient; early diagnosis and selection of appropriate treatment is needed to ensure patient longevity and retention of vital organ function.

Many previous studies [3–9] have investigated the viability of a range of prognositic biomarkers for head and neck/ oropharyngeal cancer (is oropharyngeal too different?) with varying degrees of success. The discovery of effective prognostic biomarkers has been difficult, and thus far has largely focused on immunohistochemistry techniques. Magnetic Resonance Imaging (MRI) has also been utilised [10–12] to estimate various clinical biomarkers in a non-invasive manner. However MRI based techniques often either overestimate or underestimate when attempting to quantify biomarkers when

they are evaluated using direct measurements using pathological staging sections [13, 14].

In cases where lower biological aggression is demonstrated, a de-escalation of therapy is possible [15]. Identification of these cases is paramount to minimising the adverse effects of treatment, and improving patient outcomes. Previous work [16–18] has hypothesized that tumours which may be responsive to novel therapeutic treatment may carry a distinct molecular fingerprint; the identification of which may allow for screening of patients towards appropriate treatment.

This work explores the potential efficacy of fourier transform infra-red (FTIR) microscopy in combination with a known prognositic biomarker: α-Smooth Muscle Actin (ASMA) expression, as a method of identifying cases which may be appropriate for therapeutic treatment. Previous work [4–6] has explored the efficacy of ASMA and SERPINE1 [6] as predictive variables for extra capsular spread (ECS), an important prognostic biomarker for OSCC. FTIR microscopy images taken of the same sample set will be used in order to perform a comparison to established biomarkers. ASMA expression is closely associated with the presence of activated fibroblasts, also known as *myofibroblasts* in tumour associated stroma. The degree of ASMA expression can be interrogated through the use of appropriate chemical stains, and evaluated using an optical microscope.

FTIR microscopy is a well established technique and has been utilised to investigate a range of biomedical applications in recent years [19–21]. Due to its ability to access chemical information present within the sample; analysis of FTIR microscopy data is able to lend insight into a range of label-free discrimination tasks. FTIR microscopy allows for imaging of sample specimens at a multitude of infra-red wavelengths simultaneously. This is achieved through the use of a broadband light source and Michelson interferometer set up. Individual chemical spectra are then obtained by performing a Fourier transform on the resulting interferogram. Marginal spectral differences in biochemical compounds of interest are typically located in a region known as the fingerprint region (1000cm^{-1}-1800cm^{-1}). It is differences in these absorption bands which

contain information which can be utilised to discriminate between samples of interest.

Zawlik et.al [22] investigated FTIR coupled with principal component analysis (PCA) to investigate the efficacy of chemotherapy in triple-negative breast cancer. They determined that it was possible to monitor changes in the biochemical composition of the tissue in order to monitor the effectiveness of received treatment.

Butler et.al [23] have undertaken development of a high-throughput ATR-FTIR based instrument for use in biofluid assays. Their work concluded that it was possible to utilise IR spectroscopy to triage brain cancer using biofluid samples with a sensitivity and specificity of 93.2% and 92.8% respectively.

2 Materials and Methods

Tissue preparation

The dataset is comprised of FTIR spectra taken from primary tumour sites of 29 patients with a diagnosis of OSCC. The specimens are a subset of those arranged in a previously described tissue microarray (TMA; [6]). Inclusion criteria for this study were: a diagnosis of OSCC; the presence of OSCC in the TMA core (see below); the ability to co-register adjacent H&E stained and FTIR imaged sections (see below); a follow-up period after surgery of at least 24 months [check]. Patients gave informed consent and the study was undertaken under ethical approval (Northwest - Liverpool Central REC number EC47.01). All samples were 1mm diameter cores of formalin fixed paraffin embedded (FFPE) taken from a tissue micro array (TMA).

Four adjacent sections of 4μm thickness were taken from the TMA, the first and last sections were stained with Haematoxylin and Eosin (H&E) and used to assess the presence and location of tumour material in the 2nd and 3rd sections. Specimens were removed from the sample set if no clear area containing mostly tumour cells was discernable in the H&E stained sections. Samples were also removed from the sample

set if the outline of the regions containing tumour cells were markedly different between the 1st and 4th sections. Images of stained sections were scanned using an Aperio CS2 scanner (Leica Biosystems) and used for IR image annotation. The 2nd and 3rd TMA sections were mounted onto CaF_2 disks for FTIR microspectroscopy.

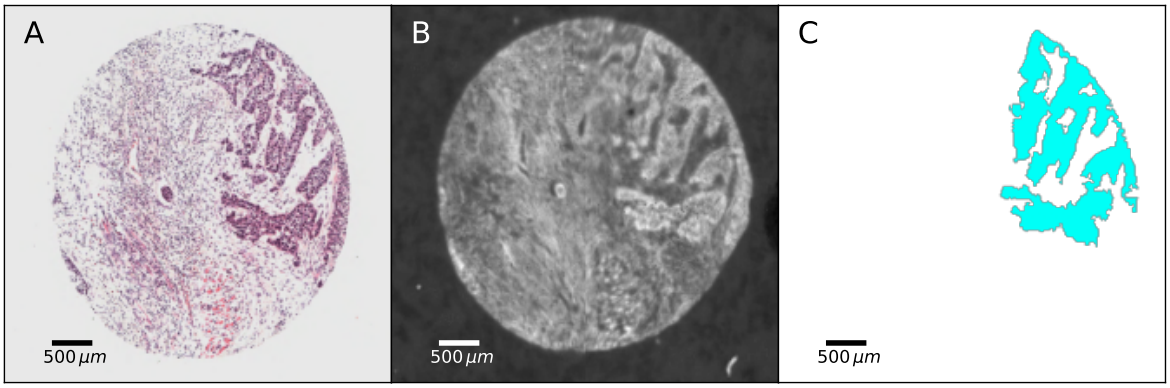

Figure 1: Annotation of OSCC-containing areas in FTIR images. A: H&E image of a tissue core; B: FTIR image at 1650cm^{-1}; C: Areas from which FTIR data was extracted for analysis

pt selection: diag of sqOSCC; co-registration of H&E and IR; presence of OSCC in 1 4 ¡¡— Ask Janet

FTIR Microspectroscopy

FTIR measurements of TMA cores were taken at room temperature using a Varian Cary 670-FTIR spectrometer with an attached Varian Cary 620-FTIR microscope produced by Varian (now Agilent Technologies, Santa Clara CA, USA); with a liquid nitrogen cooled 128×128 pixel mercury-cadmium-telluride (MCT) focal plane array with an effective field of view for each pixel of 5.5µm. The sample stage was enclosed in a perspex box and pumped with dry air until a humidity of 1% was achieved into order to mitigate the effects of water contributions on measured IR spectra. Images were acquired at a resolution of 6cm^{-1} over a spectral range of 990cm^{-1} to 3800cm^{-1} using a co-addition of 128 scans. Attenuator and integration time of the FPA were chosen to gain the maximum signal-to-noise ratio. Background scans were acquired using a blank CaF_2 disk situated within the perspex box before each session of measurements.

Data Preprocessing & Analysis

Selection of tissue areas to include in the analysis ~~annotation~~ was undertaken by a ~~maxillofacial~~ pathologist (AT), who identified regions containing high proportions of tumour cells on the H&E images. These were subsequently co-registered with IR images at 1650cm^{-1} (the amide-I peak), from the same tissue core in order to target extraction of IR data for analysis ~~(Figure 1).~~

In order to correct for atmospheric scattering, extracted spectra were pre-processed using an open-source extended multiplicative scattering correction (EMSC) code provided by Kohler et.al [24]. A number of preprocessing steps were carried out on the dataset before a final classification step was performed using a logistic regression (LR) classifier. An unsupervised quality control check of all data was used to eliminate anomalous spectra through the use of the multivariate Hotelling's T^2 statistic [25, 26]. Spectra determined to have a T^2 value lying outside the 95^{th} percentile were deemed to be anomalous and were omitted from further analysis.

Vector normalisation was used in order to account for sample thickness; wavenumber absorbance features were zero-centered~~,~~ and variance scaled to one before a final principal component analysis (PCA) step to reduce dimensionality of the dataset. Seven principal components were taken ~~to consider only those of greatest variance and~~ to assist convergence when fitting the LR classifier. A large regularisation penalty was applied when fitting the LR model, to mitigate the possibility of overfitting.

~~A number of~~ scientific Python packages [27–29] were used to implement ~~all~~ classification models and survival analysis. The classification power of an FTIR spectrum as a biomarker was estimated using the AUC of the receiver operating characteristic (ROC) curve, and a precision-recall (PR) curve. In order to obtain an estimate of the variability of the classification power of FTIR, bootstrap out-of-bag sampling was utilised. A training data set was constructed by drawing 80% of patients in the total dataset without replacement. The remaining 20% was used as the "out of bag" test set on which fitted models were evaluated, and statistics calculated. This process

was repeated 100 times ensuring that no two sample sets were identical. When fitting the LR model, data points were weighted to compensate for differing number of acquired spectra per patient and to mitigate the effect of class-imbalance on classification scores. Calculated statistics included: AUC, Matthews correlation coefficient (MCC), specificity, sensitivity, positive predictive value (PPV), and negative predictive value (NPV). Prognostic efficacy was investigated using Kaplan-Meier survival-analysis, a Cox proportional hazards regression, and a log-rank test.

Prediction of patient outcomes

To facilitate improved clinical decision making, it was decided to stratify the cohort into "high" and "low" risk categories. The choice of risk group for each patient was determined through an optimisation routine which maximised the log-rank statistic with respect to the groupings of patients. The optimisation procedure was performed using a genetic algorithm (GA) based approach utilising the distributed evolutionary algorithms for python (DEAP) library [30].

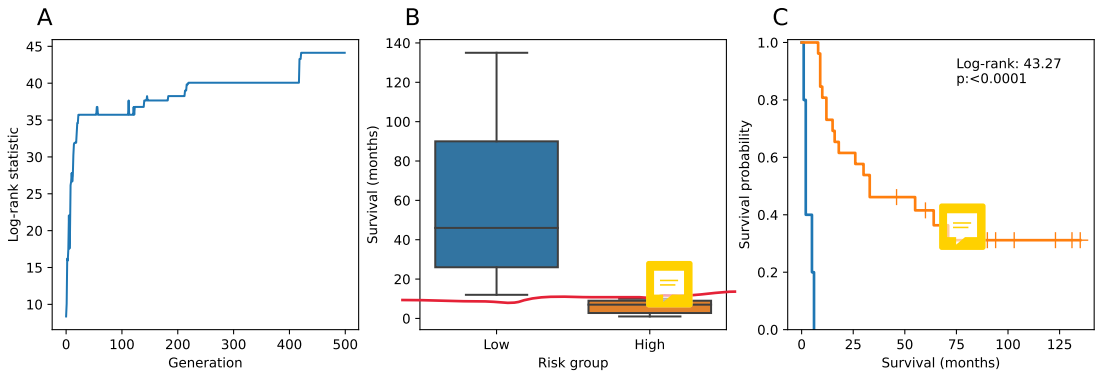

Figure 2: A: Maximum log-rank statistic vs GA generation plateauing around 40. B: box plots of survival duration in each risk group.

~~Figure 2 A shows the max fitness (in this case the log-rank statistic) of all individuals in the generation against the generation number. The best achieved value converges around 45; the patient risk groupings corresponding to the best value is taken as the optimal way of grouping the cohort into two groups.~~

3 Results

The inclusion criteria designated in materials and methods gave a sample set of 29 patients from the original 102 previously described [6]. The cohort was representative of this original patient set except that the male:female ratio was inverted (table 1). In agreement with the published cohort, our sample set was enriched for cases with extra-capsular spread (i.e. poor prognosis) in comparison to the general HNSCC population [31]. Of these 29 patients, 19 remained alive 12 months after surgery, while 14 survived to two years.

Table 1: Clinicopathological and outcome data of the current cohort

	All (N=31)	Outcome at 12 months		Outcome at 24 months		Original cohort [6]	Larger, local cohort [31]
		Dead	Alive	Dead	Alive	N=102	N=489
Age (years)							
Mean	60	70.4	56.3	64.5	57.2	60	
Range	29-85	59-85	29-72	48-85	29-68	29-89	
Median	61	70.5	56.5	64	60		
α-SMA							
High/Intermediate	26 (94)						
Low	3 (6)						
Gender							
F	7 (24)†	0	7	2	6	57 (56)[a]	187 (38)[b]
M	22 (76)	10	12	13	10	45 (45)	302 (62)
T Stage							
1	1 (3)	0	1	0	1		123 (25)[b]
2	14 (48)	4	10	7	8		175 (35)
3	2 (7)	0	2	2	0		47 (10)
4	8 (28)	4	4	3	5		144 (30)
4a	4 (14)	2	2	2	2		
N Stage							
0	7 (24)	2	4	1	5	38 (37)[b]	314 (64)[c]
1	7 (24)	2	4	2	4	18 (17)	64 (14)
2a	1 (3)	1	0	1	0		101(20)
2b	16 (55)	4	9	8	5	45 (44)	
2c	3 (10)	1	2	3	0		
Pathological Site							
Floor of mouth	8 (28)	2	6	4	4	35 (34)[b]	162 (33)
Other	12 (41)	5	7	5	7	24 (24)	183 (36)
Tongue	9 (31)	3	6	6	3	37 (36)	144 (30)

a: $p<0.005$; b: p=NS; c: $p<0.00001$
*: T stage 1+2 v 3+4

†: numbers in parenthesis are percentages
#: N stage 0 v 1 v 2

Table 1 shows that males were more prevalent than females in this cohort. The commonest TNM stage characteristics were T2 and T4; with N2b being the most prevalent nodal metastasis status.

Prediction of death within one year

The potential of FTIR as a prognositic tool was evaluated through comparison with previous work on the same sample set [6]. Three datasets were constructed consisting of FTIR data, ASMA data, and a joint FTIR-ASMA dataset. Figure 3 shows ROC and PR curves for models using ASMA data (blue), FTIR with ASMA data (orange), and FTIR alone (green).

A total of 168,460 FTIR spectra were obtained from the 21 patients who survived beyond one year and 96,402 spectra were obtained from 10 patients who died within 12 months. After modelling these data in 100 different train/test iterations, as described in materials and methods, the final prediction score was taken to be the median of the scores predicted for each patient.

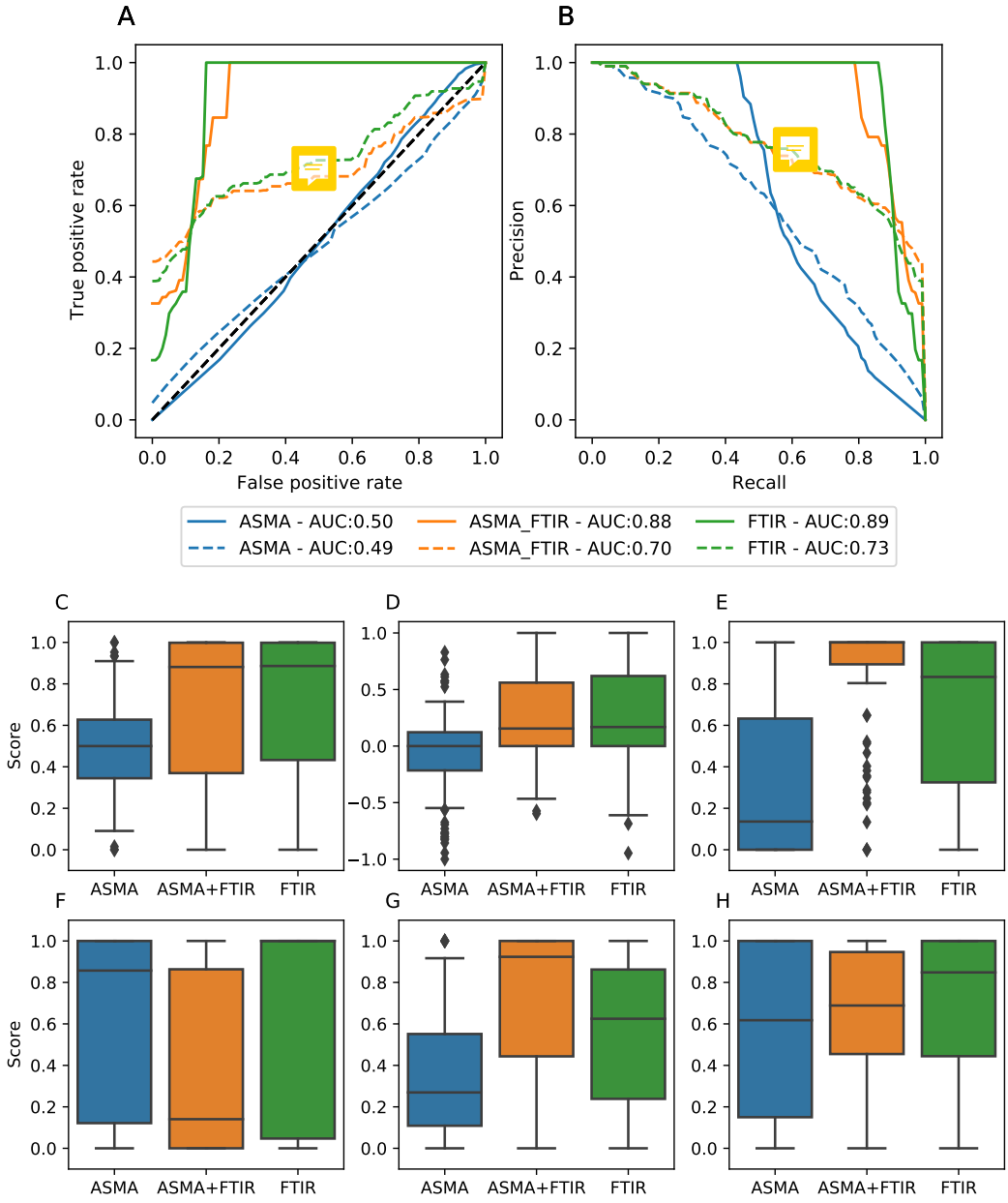

Figure 3: Median(mean) ROC and PR curves shown in solid(dashed) lines showing classification power of the prediction of risk group. AUC scores ~~are shown~~ for each set of predictive variables. Whisker boxplots of classification statistics calculated across all ~~sample subsets~~. AUC (C); MCC (D); specificity (E); sensitivity (F); PPV (G); NPV (H). Boxes show the median, 25^{th}, and 75^{th} percentiles; whiskers extend to points that lie within 1.5 inter quartile ranges of the lower and upper quartiles; points lying outside this range are shown.

The median AUC (area under the receiver operating characteristic curve) was ~~shown to be~~ 0.89 (Figure 3 A); incorporation of the ASMA data into this analysis, decreased the AUC slightly to 0.88; ASMA alone achieved a significantly poorer score of 0.5. Although the precision decreased with recall, the overall curve suggested that the data

was sufficiently balanced to accept the model (Figure 3 B). Furthermore, additional classification statistics produced comparable conclusions, showing that the model was a good predictor of poor outcome (Figure 3 C-H).

Table 2: Median classification statistics

Variables	AUC	F1	MCC	Specificity	Sensitivity	PPV	NPV
ASMA	0.5	0.24	0	0.136	0.857	0.269	0.618
ASMA + FTIR	0.881	0.562	0.155	1	0.14	0.924	0.689
FTIR	0.886	0.536	0.168	0.833	1	0.625	0.848

~~Figure 3 is a visual representation of classification metrics calculated across sample subsets for each model. Consistently high AUC scores were observed, with a median of 0.88 for both models using FTIR data. The model using ASMA along had a median AUC of 0.5.~~ Particularly good statistics were observed for the model using FTIR alone with median sensitivity and specificity at 1 and 0.83 respectively. Furthermore, the combined model also suffers from a low sensitivity and NPV in comparison to the FTIR model

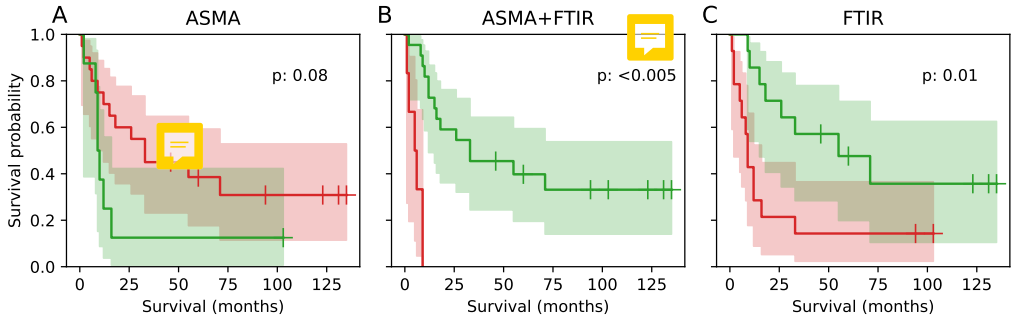

Figure 4: Kaplan-Meier survival curves for each risk group according input variables. Low-risk:green, high-risk:red

A univariate Cox's proportional hazard model was fit to median prediction scores ~~outputted by~~ the logistic model. Figure 4[A-C] survival curves for high(low) risk groups are shown in red(green) for each model. Figure 4[A] shows much overlap between risk groups with patients with a log-rank giving a non-significant p value of ¿ 0.05. Figure 4[B] shows a clear distinction between risk groups ¡0.005; indicating that the model is prognostically useful. Figure 4[C] is again significant but with less prognostic utility than the combined model.

Table 3: Cox proportional hazards model fit statistics

	coef	se(coef)	z	p	-log2(p)	Hazard ratio (HR)
ASMA	-0.078	2.26	-0.034	0.973	0.04	0.925 (0.011-77.679)
ASMA+FTIR	2.07	0.941	2.199	0.028	5.166	7.923 (1.253-50.134)
FTIR	2.017	0.973	2.073	0.038	4.71	7.516 (1.116-50.62)

Results of the Cox regression and log-rank test both show models utilising FTIR achieved a higher classification performance over the ASMA model. Table 3 shows results from the Cox regression for each set of variables. Both models using FTIR data have significantly higher hazard ratios than the pure ASMA model, suggesting that the logistic classifier is able to determine patients at higher risk.

COMMENT ON P-VALUES

4 Discussion

Results obtained here show that FTIR was proven to be capable at stratifying a patient cohort into useful clinical risk groups. Survival analysis showed that groups allocated by the classifier had significantly different outcomes. Figure 4[B] closely resembles Figure 2[C]; suggesting that the combined model can effectively reproduce the 'ideal' model presented in fig. 2[C]. Model predictions using FTIR data showed a marked improvement over the pure ASMA model. Hazard ratios of 7.9 and 7.5 for the ASMA+FTIR and FTIR model respectively, show that the prognoses of patients allocated to the high-risk group are significantly poorer.

The use of FTIR in clinical diagnostics is growing quickly, however relatively little work has been aimed towards prognostic biomarkers. The combination of both FTIR microscopy with techniques more familiar to oncologists such as immuno histo chemical (IHC) staining has the potential to improve prognostic predictive capabilities significantly as shown in this work.

Many other prognostic biomarkers exist [32–34] but a large proportion are still in the

"discovery phase" - requiring further study to ascertain prognostic benefit [35]. The use of FTIR within clinical diagnostics likely fits into this category, as many potential barriers facing other potential biomarkers are still present.

A relatively small sample set was a key issue facing this study due to the difficulty in acquiring and imaging large numbers of samples.

Despite attempts to determine the feasibility of FTIR as a prognostic tool through multiple sampling of the dataset; a larger study would likely need to be conducted in the future, to estimate wider clinical utility.

5 Conclusion

The use of FTIR in a clinical setting is still in its infancy, however the work covered here shows that it has the potential to be of significant benefit as a prognostic tool. The addition of ASMA information was shown to be beneficial in one case, and demonstrates that additional information from other modalities could lead to the creation of a novel and informative prognostic tool. In order to progress the work covered here a larger patient sample set would be needed to affirm the conclusions reached here. The addition of information from a broader range IHC stains or imaging modalities could further increase the prognostic benefit outlined here and yield powerful tools for clinicians.

References

[1] Carla Conti et al. "Microimaging FTIR of head and neck tumors. IV". In: *Microscopy Research and Technique* 72.2 (2009), pp. 67–75. ISSN: 1059910X. DOI: 10.1002/jemt.20644.

[2] Athanassios Argiris et al. "Head and neck cancer Athanassios". In: *Lancet* 371.9625 (2008), pp. 1695–1709. DOI: 10.1016/S0140-6736(08)60728-X.Head.

[3] David Chin et al. “Novel markers for poor prognosis in head and neck cancer”. In: *International Journal of Cancer* 113.5 (2005), pp. 789–797. ISSN: 00207136. DOI: 10.1002/ijc.20608.

[4] M. G. Kellermann et al. “Myofibroblasts in the stroma of oral squamous cell carcinoma are associated with poor prognosis [3]”. In: *Histopathology* 51.6 (2007), pp. 849–853. ISSN: 03090167. DOI: 10.1111/j.1365-2559.2007.02873.x.

[5] Marilena Vered et al. “Tumor-host histopathologic variables, stromal myofibroblasts and risk score, are significantly associated with recurrent disease in tongue cancer”. In: *Cancer Science* 101.1 (2010), pp. 274–280. ISSN: 13479032. DOI: 10.1111/j.1349-7006.2009.01357.x.

[6] J Dhanda et al. “SERPINE1 and SMA expression at the invasive front predict extracapsular spread and survival in oral squamous cell carcinoma”. In: August (2014), pp. 2114–2121. ISSN: 0007-0920. DOI: 10.1038/bjc.2014.500.

[7] Chun Ta Liao et al. “Pathological risk factors stratification in pN3b oral cavity squamous cell carcinoma: Focus on the number of positive nodes and extranodal extension”. In: *Oral Oncology* 86.September (2018), pp. 188–194. ISSN: 18790593. DOI: 10.1016/j.oraloncology.2018.09.021. URL: https://doi.org/10.1016/j.oraloncology.2018.09.021.

[8] Corey C. Foster et al. “Dose and Volume De-Escalation for Human Papillomavirus–Positive Oropharyngeal Cancer is Associated with Favorable Posttreatment Functional Outcomes”. In: *International Journal of Radiation Oncology Biology Physics* 107.4 (2020), pp. 662–671. ISSN: 1879355X. DOI: 10.1016/j.ijrobp.2020.04.014. URL: https://doi.org/10.1016/j.ijrobp.2020.04.014.

[9] Gerard Mamelle et al. “Lymph node prognostic factors in head and neck squamous cell carcinomas”. In: *The American Journal of Surgery* 168.5 (1994), pp. 494–498. ISSN: 00029610. DOI: 10.1016/S0002-9610(05)80109-6.

[10] Christine T. Lwin et al. “Accuracy of MRI in prediction of tumour thickness and nodal stage in oral squamous cell carcinoma”. In: *Oral Oncology* 48.2 (2012), pp. 149–154. ISSN: 13688375. DOI: 10.1016/j.oraloncology.2011.11.002. URL: http://dx.doi.org/10.1016/j.oraloncology.2011.11.002.

[11] Peng Wang et al. “An approach to identify, from DCE MRI, significant subvolumes of tumors related to outcomes in advanced head-and-neck cancer”. In: *Medical Physics* 39.8 (2012), pp. 5277–5285. ISSN: 00942405. DOI: 10.1118/1.4737022.

[12] Tobias Waech et al. “Measurement variations of MRI and CT in the assessment of tumor depth of invasion in oral cancer: A retrospective study”. In: *European Journal of Radiology* 135 (2021). ISSN: 18727727. DOI: 10.1016/j.ejrad.2020.109480.

[13] Jenny K. Hoang et al. “Evaluation of cervical lymph nodes in head and neck cancer with CT and MRI: Tips, traps, and a systematic approach”. In: *American Journal of Roentgenology* 200.1 (2013), pp. 17–25. ISSN: 0361803X. DOI: 10.2214/AJR.12.8960.

[14] Ming Hui Mao et al. “Accuracy of magnetic resonance imaging in evaluating the depth of invasion of tongue cancer. A prospective cohort study”. In: *Oral Oncology* 91.October 2018 (2019), pp. 79–84. ISSN: 18790593. DOI: 10.1016/j.oraloncology.2019.01.021. URL: https://doi.org/10.1016/j.oraloncology.2019.01.021.

[15] Conor P. Barry et al. “De-escalation of surgery for early oral cancer-is it oncologically safe?” In: *British Journal of Oral and Maxillofacial Surgery* 51.1 (2013), pp. 30–36. ISSN: 15321940. DOI: 10.1016/j.bjoms.2012.02.014. URL: http://dx.doi.org/10.1016/j.bjoms.2012.02.014.

[16] Rebekah K. O’Donnell et al. “Gene expression signature predicts lymphatic metastasis in squamous cell carcinoma of the oral cavity”. In: *Oncogene* 24.7 (2005), pp. 1244–1251. ISSN: 09509232. DOI: 10.1038/sj.onc.1208285.

[17] Paul Roepman et al. “An expression profile for diagnosis of lymph node metastases from primary head and neck squamous cell carcinomas”. In: *Nature Genetics* 37.2 (2005), pp. 182–186. ISSN: 10614036. DOI: 10.1038/ng1502.

[18] D. S. Rickman et al. “Prediction of future metastasis and molecular characterization of head and neck squamous-cell carcinoma based on transcriptome and genome analysis by microarrays”. In: *Oncogene* 27.51 (2008), pp. 6607–6622. ISSN: 09509232. DOI: 10.1038/onc.2008.251.

[19] Alexandra Sala et al. “Biofluid diagnostics by FTIR spectroscopy: A platform technology for cancer detection”. In: *Cancer Letters* 477.December 2019 (2020), pp. 122–130. ISSN: 18727980. DOI: 10.1016/j.canlet.2020.02.020. URL: https://doi.org/10.1016/j.canlet.2020.02.020.

[20] Vera E. Sitnikova et al. “Breast cancer detection by ATR-FTIR spectroscopy of blood serum and multivariate data-analysis”. In: *Talanta* 214.October 2019 (2020), p. 120857. ISSN: 00399140. DOI: 10.1016/j.talanta.2020.120857. URL: https://doi.org/10.1016/j.talanta.2020.120857.

[21] Daniela Lazaro-Pacheco et al. “Deciphering the structural and chemical composition of breast cancer using FTIR spectroscopy”. In: *Applied Spectroscopy Reviews* 0.0 (2020), pp. 1–15. ISSN: 0570-4928. DOI: 10.1080/05704928.2020.1843471. URL: https://doi.org/10.1080/05704928.2020.1843471.

[22] Izabela Zawlik et al. “FPA-FTIR Microspectroscopy for Monitoring Chemotherapy Efficacy in Triple-Negative Breast Cancer”. In: *Scientific Reports* 6 (2016), pp. 1–8. ISSN: 20452322. DOI: 10.1038/srep37333.

[23] Holly J. Butler et al. “Development of high-throughput ATR-FTIR technology for rapid triage of brain cancer”. In: *Nature Communications* 10.1 (2019), pp. 1–9. ISSN: 20411723. DOI: 10.1038/s41467-019-12527-5. URL: http://dx.doi.org/10.1038/s41467-019-12527-5.

[24] A. Köhler et al. “Estimating and correcting Mie scattering in synchrotron-based microscopic fourier transform infrared spectra by extended multiplicative signal

correction". In: *Applied Spectroscopy* 62.3 (2008), pp. 259–266. ISSN: 00037028. DOI: 10.1366/000370208783759669.

[25] Pitard F.F. "An Introduction to the Theory of Sampling: An Essential Part of Total Quality Management". In: *Comprehensive Chemometrics* (2009), pp. 1–16. URL: http://www.sciencedirect.com/science/article/pii/B9780444527011000892.

[26] Wolfgang Karl Härdle and Léopold Simar. *Applied multivariate statistical analysis, fourth edition*. 2015, pp. 1–580. ISBN: 9783662451717. DOI: 10.1007/978-3-662-45171-7.

[27] F. Pedregosa et al. "Scikit-learn: Machine Learning in Python". In: *Journal of Machine Learning Research* 12 (2011), pp. 2825–2830.

[28] Cameron Davidson-Pilon. "lifelines: survival analysis in Python". In: *Journal of Open Source Software* 4.40 (2019), p. 1317.

[29] Pauli Virtanen et al. "SciPy 1.0: Fundamental Algorithms for Scientific Computing in Python". In: *Nature Methods* 17 (2020), pp. 261–272. DOI: 10.1038/s41592-019-0686-2.

[30] Félix-Antoine Fortin et al. "DEAP: Evolutionary Algorithms Made Easy". In: *Journal of Machine Learning Research* 13 (July 2012), pp. 2171–2175.

[31] Simon N. Rogers et al. "Survival following primary surgery for oral cancer". In: *Oral Oncology* 45.3 (2009), pp. 201–211. ISSN: 13688375. DOI: 10.1016/j.oraloncology.2008.05.008. URL: http://dx.doi.org/10.1016/j.oraloncology.2008.05.008.

[32] J Zapała et al. "Proliferative index activity in oral squamous cell carcinoma : indication for postoperative radiotherapy ?" In: (2014), pp. 1189–1194. DOI: 10.1016/j.ijom.2014.03.013.

[33] Thomas Scholzen and Johannes Gerdes. "The Ki-67 Protein : From the Known and". In: 322.August 1999 (2000), pp. 311–322.

[34] Neelam G Shah et al. “Prognostic significance of molecular markers in oral squamous cell carcinoma : a multivariate analysis”. In: December (2009), pp. 1544–1556. DOI: 10.1002/hed.

[35] César Rivera et al. “Prognostic biomarkers in oral squamous cell carcinoma: A systematic review”. In: *Oral Oncology* 72 (2017), pp. 38–47. ISSN: 18790593. DOI: 10.1016/j.oraloncology.2017.07.003.